Chapter 2

Photonic Crystal Fiber–Based Interferometric Sensors

Dora Juan Juan Hu, Rebecca Yen-Ni Wong and
Perry Ping Shum

Additional information is available at the end of the chapter

http://dx.doi.org/10.5772/intechopen.70713

Abstract

Photonic crystal fibers (PCFs), also known as microstructured optical fibers, are a highlighted invention of optical fiber technology which have unveiled a new domain of manipulating light in engineered fiber waveguides with unparalleled flexibility and controllability. Since the report of the first fabricated PCF in 1996, research in PCFs has resulted in numerous explorations, development and commercialization of PCF-based technologies and applications. PCFs contain axially aligned air channels which provide a large degree of freedom in design to achieve a variety of peculiar properties; numerous PCF-based sensors have been proposed, developed and demonstrated for a broad range of sensing applications. In this chapter, we will review the field of research on design, development and experimental achievement of PCF-based interferometric sensors for physical and biomedical sensing applications.

Keywords: photonic crystal fibers, interferometry, fiber optic sensors, Fabry-Perot interferometer, Mach-Zehnder interferometer, Michelson interferometer, Sagnac interferometer

1. Background

Optical fiber interferometric sensors have been widely used for various sensing applications and characterization of physical magnitudes. The advantages provided by optical fibers have been well recognized and utilized in interferometric sensor applications, which include compactness, alignment freedom from free space optics, high sensitivity, high reliability etc. [1]. Photonics crystal fibers (PCFs), a highlighted fiber technology that was first invented and demonstrated in 1996, have brought breakthroughs in communications, sensing, defense and medicine [2]. These fibers have demonstrated superior features in many applications and created substantial scientific and industrial impact in recent years. In the past decade, PCFs have received intensive and continuous attention, and undergone rapid development from

design and fabrication to device realization and commercialization. Compared to conventional optical fibers, PCFs represent a more versatile platform to construct interferometry sensors because of enhanced flexibility in manipulating optical properties and light-medium interactions. Various PCF structures, such as polarization-maintaining (PM) PCFs, photonic bandgap (PBG) PCFs including hollow core (HC) PCFs and all-solid PBG PCFs, Bragg fibers, large mode area (LMA) PCFs and highly nonlinear PCFs have been demonstrated with good potential in developing interferometric fiber sensors. PCFs can provide a platform for integration of materials such as gas, fluid or metals for additional functionality. For example, PCFs have been exploited for optofluidic sensing and gas sensing applications utilizing the selective or unselective infiltration of fluid or gas in the holey structures [3]. In addition, they are a desirable platform for the incorporation of plasmonic structures that can enhance application opportunities in terms of performance as well as versatility. Integration of plasmonic structures such as metal nanoparticles, metal nanowires, and metal thin films in PCF structures have proven to substantially improve sensor performance, e.g. sensitivity [4]. The continuing development and maturation of PCF technologies and PCF-based interferometric sensors are expected to make more contributions to optical fiber technology and real world applications [5].

2. Overview of PCF-based interferometric sensors

In this chapter, various configurations of interferometry sensors based on PCFs and their sensing applications are demonstrated, namely Fabry-Perot interferometer (FPI), Mach Zehnder interferometer (MZI), Michelson interferometer and Sagnac interferometer. Compared to standard optical fibers, PCF structures possess many interesting characteristics and tunable properties which are highly desirable when constructing interferometric sensors with enhanced performance.

2.1. Fabry-Perot interferometer (FPI)

A Fabry-Perot interferometer is comprised of a cavity (or etalon) made of two highly reflective surfaces/mirrors which enable light propagating down the fiber to be partially reflected. The transmitted, and subsequently, reflected beams will form an interference pattern due to the difference in phase delay.

The reflection coefficients, R_i, at the mirrors can be defined by [6]:

$$R_i = \left(\frac{n_i - n_{i+1}}{n_i + n_{i+1}}\right)^2, i = 1, 2, 3, \ldots \tag{1}$$

where n_i is the refractive index of the cavity and surrounding medium.

The phase difference, δ, of the interferometer can be represented by [1]:

$$\delta = \frac{2\pi}{\lambda} n2L \tag{2}$$

where λ is the incident light wavelength and L is the physical length of the cavity.

FPIs can typically be classed as either extrinsic or intrinsic, depending on their make-up. Extrinsic FPIs (EFPI), as shown in **Figure 1(a)**, use the air gap between two fibers and reflects light between the cleaved ends. The cavity of intrinsic FPIs (IFPI) is formed within the fiber itself, where the two reflectors lie along the length of the fiber [1], as shown in **Figure 1(b), (c)**. IFPIs can have advantages over EFPIs such as higher coupling efficiency.

For IFPIs, the etalon/cavity can be formed by fusion splicing a section of HC-PCF, which acts as the cavity, between two lengths of single mode fiber with cleaved end surfaces [7]. This configuration allows for a customizable cavity length, which can be a few micrometers or a few centimeters long [7]. Villatoro . presented a spherical FP cavity by means of a microscopic air bubbles (20–58 μm diameters) fabricated via arc discharge between a standard SMF and a PCF. This technique can reduce the number of steps required for fabricating FPIs [8]. Favero et al. [9] pressurized the holes in the PCF to produce reproducible elliptical bubbles with controllable cavity dimensions.

Hu et al. [6] were able to realize a refractive index tip sensor used in reflection mode. This sensor was based on a hollow silica sphere with a thin silica wall being formed at one end of a simplified HCF via means of arc discharge, as shown in **Figure 2**. The reflected spectrum was modulated by the interaction between the sensor head and the environment (refractive index (RI) and temperature). A RI resolution of 6.2×10^{-5}, using fringe visibility (**Figure 2 (c)**), was determined and the temperature sensitivity for the high and low frequency fringes were 1.3 and 17 pm/°C, respectively (**Figure 2 (d)**), at temperatures up to ~1000°C.

Micro FP cavities can offer low cross sensitivity with temperature, yet high RI sensitivity. A RI sensor was realized by drilling micro-holes into a simplified hollow core (SHC) PCF micro

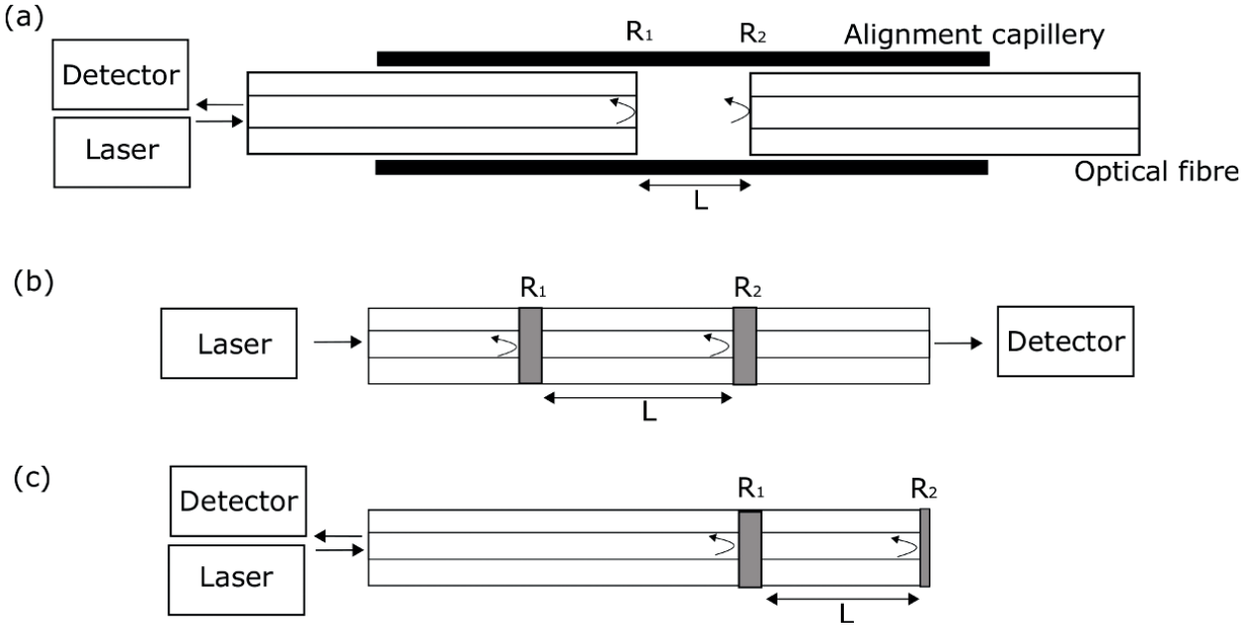

Figure 1. (a) The schematic of an extrinsic Fabry-Perot interferometer; (b) the schematic of an intrinsic Fabry-Perot interferometer; (c) the schematic of an intrinsic Fabry-Perot interferometer working in reflection mode. R_i represents the reflective surfaces and L is the length of the cavity.

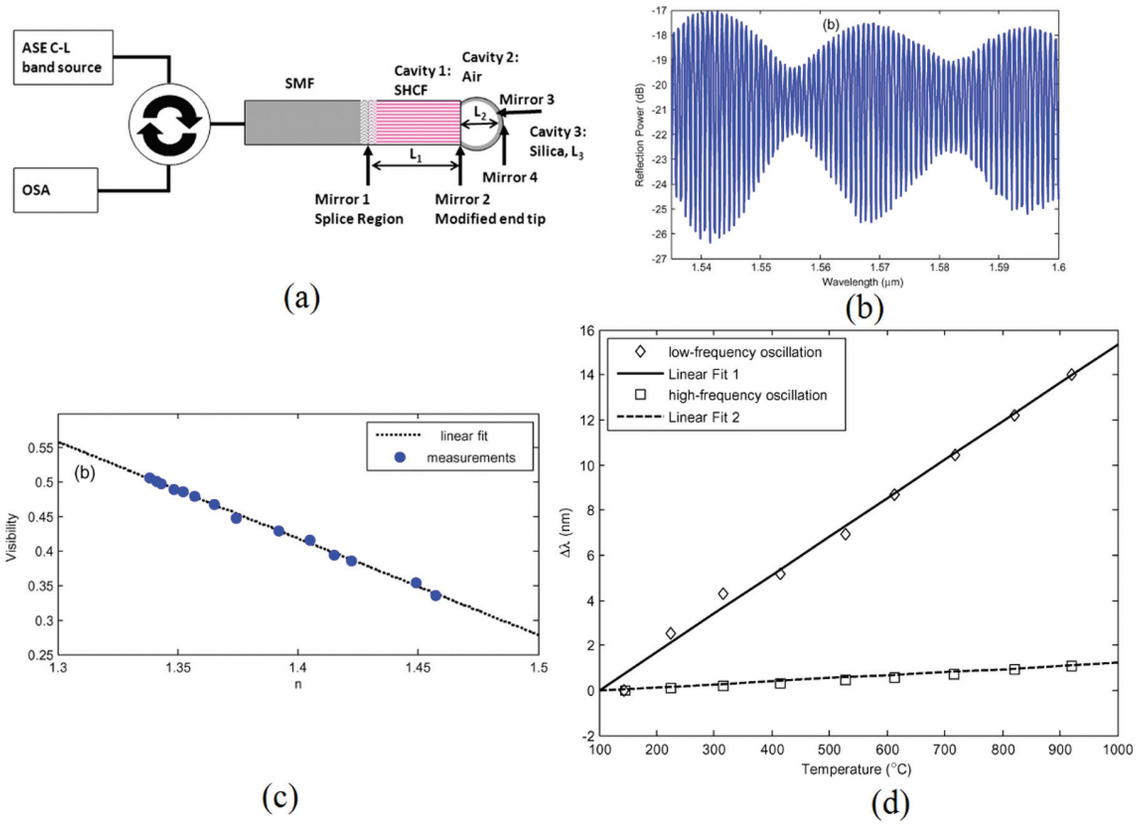

Figure 2. (a) Configuration of the simplified HCF based IFPI working in reflection mode; (b) interference spectrum of the sensor head; (c) refractive index against fringe visibility. (d) Temperature sensitivity against wavelength shift for low and high frequency oscillations. © 2012 IEEE. Reprinted, with permission, from Ref. [6].

cavity using a femtosecond laser to allow the analyte to enter the cavity [10]. A RI sensitivity of ~851 nm/RIU and a low cross sensitivity with temperature of ~3.2 × 10^{-7} RIU/°C was obtained. A short section of hollow fiber had been sandwiched between single mode fiber (SMF) and solid core (SC) PCF [11]. By taking advantage of the air holes in PCF, air was allowed to infiltrate the PCF cavity and the RI changes under different pressures were measured. When creating hole collapse regions between a section of SMF and PCF, the length of the region can affect the sensitivity of the sensor to RI and also temperature. A longer collapsed area will lead to more cladding modes being excited and in turn larger changes in the interference pattern. Dash and Jha [12] found that as they increased the length of the collapsed region from 180 to 270 μm, the RI sensitivity also increased from 30 to 53 nm/RIU with a RI resolution of 1.18 × 10^{-4} RIU.

A Microbubble FPI has been shown as a strain and vibration sensor with a spheroidal cavity achieving a strain sensitivity of ~10.3 pm/με and high fringe visibility (~38 dB) [13]. A 157 nm laser was used for micromachining an in-line etalon, with two smooth and parallel reflecting sides, in an endlessly single mode PCF. This was demonstrated for strain measurements in a high temperature environment with a fringe contrast of ~26 dB [14]. Shi et al. [15] were able to produce a multiplexed strain sensor system using different lengths of HCF spliced between SMF. Due to their wide free spectral range, the signals could be easily demodulated using fast Fourier transform (FFT). A strain insensitive IFPI has been developed by splicing one end of a

solid PCF to a SMF and the other end to a HC-PCF to form a micro cavity. A large portion of the strain sensitivity comes from changing the size of the micro cavity, but in this case, this was at the end of the sensor and remained fixed in size [12].

Due to the all silica structure of PCFs, they are able to withstand high temperatures [6, 16], often for long periods of time [17]. The sensitivity to temperature is often based on the thermal-optic effect of silica and is therefore proportional to the length of the PCF cavity [18]. Frazão et al. [18] characterized the strain and temperature sensitivities of suspended core fibers with three and four holes. The normalized temperature sensitivities were found to be similar at 67.8 and 67.6 rad/m°C for three and four holes, respectively. The strain response was found to be greater for the three hole fiber. This was because the strain was applied to the cladding region (supporting walls of the fiber), and this cross-section was smaller for the three hole fiber.

Wu et al. were able to successfully demonstrate a high pressure (up to 40 MPa) and high temperature FPI (up to 700°C) sensor. A SC-PCF was spliced to one end to a SMF and hole collapse was carried out at the other end, to improve the reflectivity of the second mirror. The pressure and temperature sensitivities were −5.8 and ~13 pm/°C, respectively [19]. PCF based IFPIs may also have potential use in photonic integrated circuits [20].

2.2. Mach-Zehnder interferometer (MZI)

The Mach-Zehnder interferometer (MZI) works where an incident beam from a single light source is split into two arms and later recombined, forming an interference pattern [1]. When there is a perturbation in one arm, the difference in optical path length changes and is conveyed by the variation in the interference signal.

A MZI can be fabricated using two fibers with the light being split and recombined using fiber couplers, as shown in **Figure 3(a)**. One beam is referred to as the reference arm, and the other the sensing arm. To fabricate an in-line MZI using a singular fiber, as in **Figure 3(b)**, modal dispersion is used and the propagating modes are coupled into the cladding as well as the core. Though the physical length of the two arms is the same the phase velocity is different as the effective indices of the core and cladding are not the same.

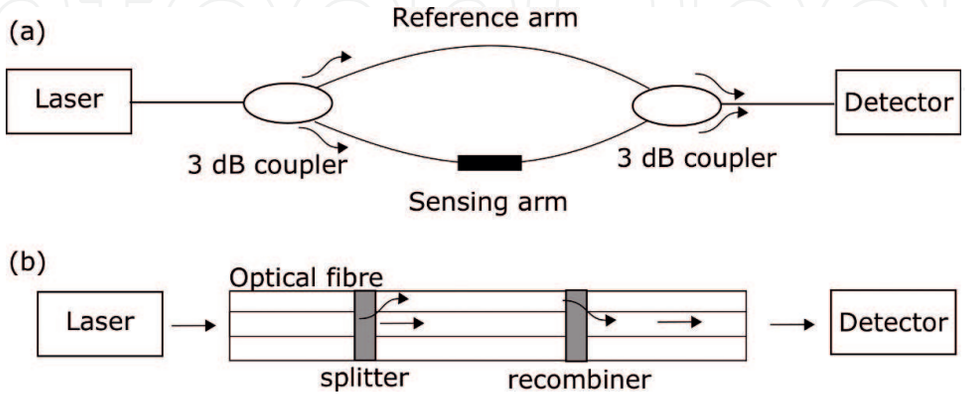

Figure 3. (a) The schematic of a Mach-Zehnder interferometer using two fibers; (b) the schematic of an in-line Mach-Zehnder interferometer using one fiber.

The Mach-Zehnder sensor interference spectrum can be expressed as [21]:

$$I = I_1 + I_2 + 2\sqrt{I_1 I_2}\cos\Delta\varnothing \tag{3}$$

where I_1 and I_2 are the irradiance of the interfering waves, $\Delta\varnothing$ is the phase difference between the core and cladding mode is defined as:

$$\Delta\varnothing = \frac{2\pi}{\lambda}\Delta nL + \Phi \tag{4}$$

where λ is the wavelength, L is the optical length of the interferometer, Δn is the difference in effective refractive index and Φ is the initial phase difference of the two waves.

PCF MZIs commonly consist of a SMF-PCF-SMF configuration; where a small section of solid core PCF is spliced between two standard SMFs. By using a fusion splicer to collapse the air holes of the PCF, the light is no longer constrained to the core and some of the light is coupled to one or multiple cladding modes and are able to propagate along the fiber [22, 23]. The splice points act as the mode couplers to form the fiber MZI, where the first splice point causes light from the core to couple to the cladding and the second splice causes the modes to recombine. MZIs composed entirely of LMA-PCF have also been realized [22] by core misalignment or by hole collapsing, as shown in **Figure 4**. By using the hole collapse technique in an all PCF MZI, alignment is less stringent as no cleaving is required. More cladding modes will also be excited and when the interference spectra were Fourier transformed, multiple spatial frequencies were seen with the number increasing with increasing interferometer length [22]. Different lengths of PCF were studied and compared for sensitivity [23–25]. It was found that the sensitivity was

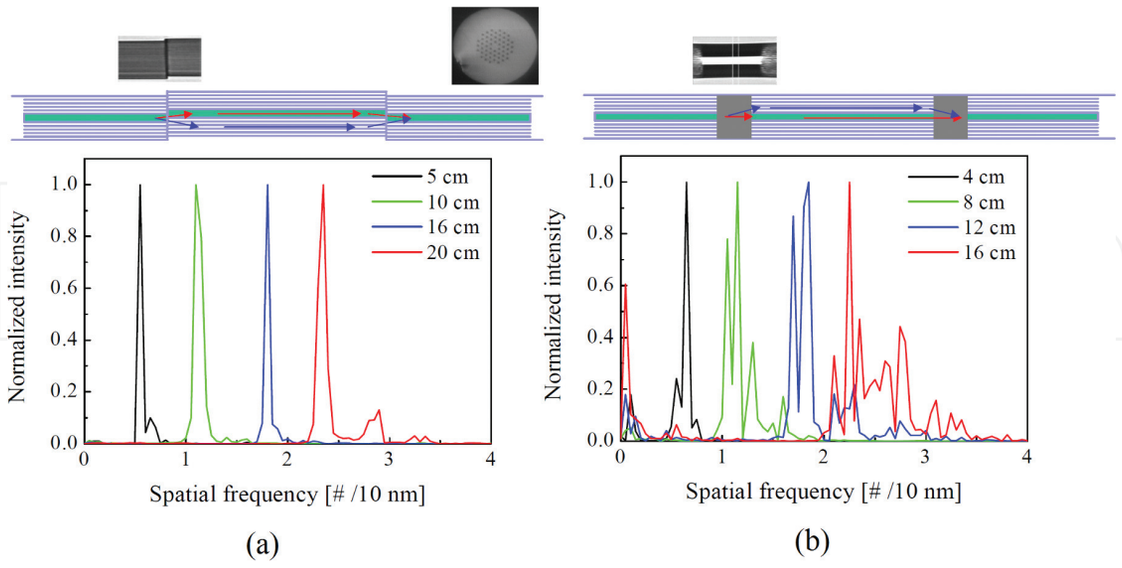

Figure 4. (a) The offset splicing method and the corresponding spatial frequencies at different interferometer lengths. Inset: Cross section of the LMA-PCF; (b) the hole collapse method and the corresponding spatial frequencies at different interferometer lengths. (a) produced one dominant spatial frequency at each length, whereas (b) induced several. Reprinted with permission from Ref. [22]. Copyright 2007 Optical Society of America.

not strongly dependent on length, though longer sections could require better handling and packaging.

These MZI configurations make useful refractometers as the effective refractive index of the cladding modes will be influenced by the surrounding environment [21, 23]. Highly sensitive refractometers have been demonstrated by means of tapering, either at just the splice points [26, 27] or the entire PCF section [28] to expose the evanescent field, making the MZI more sensitive to external RI changes. By tapering at the splice point, when compared to direct splicing, Wang et al. [27] was able to increase the sensor sensitivity from 224.2 to 260.8 nm/RIU. Wong et al. [29] used a combination of PCF-MZI and cavity ring-down technique for signal demodulation, which lead to a minimum detectable RI to be 7.8×10^{-5} RIU, almost 2.5 times greater than when compared to a PCF-MZI based on wavelength demodulation.

PCFs are generally known to be relatively temperature insensitive due to their small thermo-optic coefficient. Methods used to increase this sensitivity include, partial [30] or full [31] liquid infiltration into the holey region of the PCF, and multipath (more than two) MZIs using multicore PCFs [32] as this improves the phase sensitivity. Zhao et al. were able to achieve a temperature sensitivity of 130.6 pm/°C [32].

Different PCF configurations have been used for measuring strain [25, 33–35]. By using a multimode PCF, and careful hole collapse during splicing, a MZI was realized by coupling to two different core modes, LP_{01} and LP_{31}, allowing the light to be confined within the core and not as susceptible to ambient environment. Zheng et al. [25] were able to demonstrate a temperature and RI insensitive strain sensor with a sensitivity of 2.1 pm/με at 1550 nm with a 45 mm long PCF between two lengths of SMF. By introducing an additional collapsed region in the center of the length of PCF, two cascaded MZIs were created; the extinction ratio of the MZI induced fringes and in turn the measurement accuracy was improved [34]. The sensitivities for a normal SMF-PCF-SMF MZI and the modified MZI were 1.87 and 11.22 dB/mε, respectively. With twin core (TC) PCFs, the two cores can each act as the arm of the interferometer [36] and allow for a large strain measurement range as there are no deformations in the PCF to weaken the structure [33].

TC-PCFs have also been successfully demonstrated for use as intensity-based bend sensors [36], with a signal change found when the fiber is bent, such that both cores will experience different bend radii. Sun et al. [37] proposed a sensitive bend sensor by introducing an up- or peanut like -taper as the splitter and a down-taper as the recombiner. The up-taper improves the coupling between the PCF core and cladding modes and produces a stronger interference signal when recombined. The bend sensitivity of 50.5 nm/m^1 is one order of magnitude greater, when compared to a PCF MZI with a configuration of hole collapse and core offset (3.046 nm/m^1) [38].

The addition of a functional coating can lead to more specific and tailored sensing applications. As shown by Tao et al. [39], by coating the holey region of large mode area (LMA) and a grapefruit PCF with a polyallylamine layer with an affinity towards TNT vapor, they were able to selectively detect TNT. The LMA PCF had a lower a detection limit of 0.2 ppb_v due to a higher Q-factor. Lopez-Torres et al. demonstrated a humidity sensor capable of resolving

0.074% of relative humidity, and used a method based on the fast Fourier transform to yield a more linear device response with less noise [40]. Functionalized tip sensors have been used to detect changes in pH level [41] and changes in RI [42]. By modifying the surface of a compact PCF (~3 mm long) sensing region with biotin, Hu et al. were able to successfully demonstrate streptavidin detection [43]. Surface modified sensors can be more advantageous over air hole modification as it can be easily cleaned, reused and the analyte response is faster [43].

Long period gratings (LPGs) have also been used to fabricate in-line MZIs as they work by coupling forward propagating core light with one or more co-propagating cladding modes. This has been extended for use in all-PCF MZIs [44, 45]. Mechanically induced LPGs allow for identical, yet tuneable non-permanent LPGs to be fabricated. Yu et al. [45] demonstrated that the first LPG could be replaced by a misaligned splice point. As this is easier to manufacture than an LPG, it could reduce fabrication time and cost. The interference pattern can be tuned by adjusting the offset or the distance between the splitter and combiner [45] as well as the period and strength of the gratings [44]. It is also possible to replace the second LPG by collapsing the holes of the PCF [46]. Compact LPG based MZIs have been demonstrated, by using a CO_2 laser [35, 47] to create periodic grooves until both LPGs have coupling efficiency of around 3 dB. Compared with a standard single mode fiber MZI, Ju et al. [47] were able to obtain a higher strain sensitivity (-2.6 pm/με compared to +0.445 pm/με) and a lower temperature sensitivity (42.4 pm/°C per m compared to 1215.56 pm/°C per m). MZIs made with LPGs can be at risk of having a high insertion loss [24] due the deformation of fiber structure from inscription or from the misaligned splice point [45]. By cascading an LPG with a PCF MZI, simultaneous temperature and RI sensing was achieved as both elements in the sensor matrix responded differently to the multiple parameters [48].

Measuring low acoustic frequencies underwater can be difficult due to poor signal-to-noise ratios. An optical fiber based hydrophone using a polarization maintaining (PM) PCF sandwiched between SMFs was able to detect frequencies ranging from 5 to 200 Hz. The MZI used a two parameter detection method, namely a change in the intensity of the signal and a shift in wavelength. The change in power ranged from 0.8 to 2.32 dBm, which was much higher when compared to the ~0.1 dBm change using a SMF-MMF-SMF configuration [49].

PCF-MZIs also have potentials in communications for the demodulation of signals using differential phase shift keying (DPSK) [50] and in wavelength-division multiplexing (WDM) [51].

2.3. Michelson interferometer

Optical fiber Michelson interferometers can be realized by using two fibers or one fiber with the configurations shown in **Figure 5**. They are a similar version of MZI configurations. In the two fibers configuration, the laser light is split into two optical paths by an optical fiber coupler. The light is reflected back by the mirrors and recombined at the coupler to form the interference at the detector. In the one fiber configuration, the modes are split at a region where higher order modes or cladding modes are excited, e.g. splicing region between SMF and PCF, and are reflected by the mirrors and recombined at the splicing regions to form the interference which passes to the detector via a circulator.

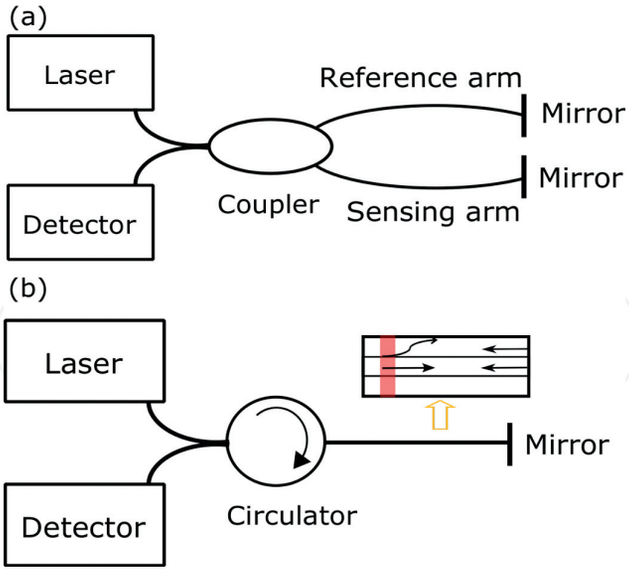

Figure 5. (a) The schematic of a Michelson interferometer using two fibers; (b) the schematic of a Michelson interferometer using one fiber.

Most PCF-based Michelson interferometers are based on one-fiber configurations. PM-PCFs have two orthogonally polarized core modes which act as two different optical paths for interference [52]. The two different optical paths can also be formed by two core modes in two-core PCFs [53, 54], or two core fibers [55]. In addition, the core mode and cladding modes that are excited at the splicing region between a SMF and a PCF due to mode mismatch [56] or a collapsed region in PCFs [57–62]. Similar configurations have also been reported in thin core fibers [63]. Due to the flexibility in the waveguide properties, PCF-based configurations can achieve high sensitivities when measuring ambient parameters, such as RI, temperature etc.

Jha et al. presented a Michelson interferometer device using a stub of a LMA PCF, with the schematic of the experimental setup and the interference spectrum in the reflected signal as shown in **Figure 6**. The PCF was fully collapsed at the splicing region between SMF and PCF, forming a multimode region for cladding mode excitation, and the end of the PCF was behaving as a reflective mirror. The dependence of the PCF length, temperature and ambient RI on the interference fringes of the device was investigated for sensing applications [58].

Enhanced temperature sensitivity was reported using a liquid-filled PCF-based Michelson interferometer [60]. The cladding holes of the PCFs were filled liquid with an RI of 1.45. The voids of the PCF were collapsed fully in the splicing process and the collapsed region between SMF and PCF was about 300 μm. The PCF end face acted as the reflective surface for the core mode and cladding modes of the PCF, which were combined and interfered in the collapsed region at the return path. The device demonstrated high temperature sensitivity with the wavelength shifts being was around 27 nm for a temperature change of 5°C [60].

Because PCF-based interferometers possess several desirable advantages including high sensitivity, linear response, and small size, they have attracted great interest in biosensing applications. Gao et al. proposed an in-line PCF Michelson interferometer for label-free, real time and sensitive detection of DNA hybridization and methylation [61]. To fabricate the interferometer,

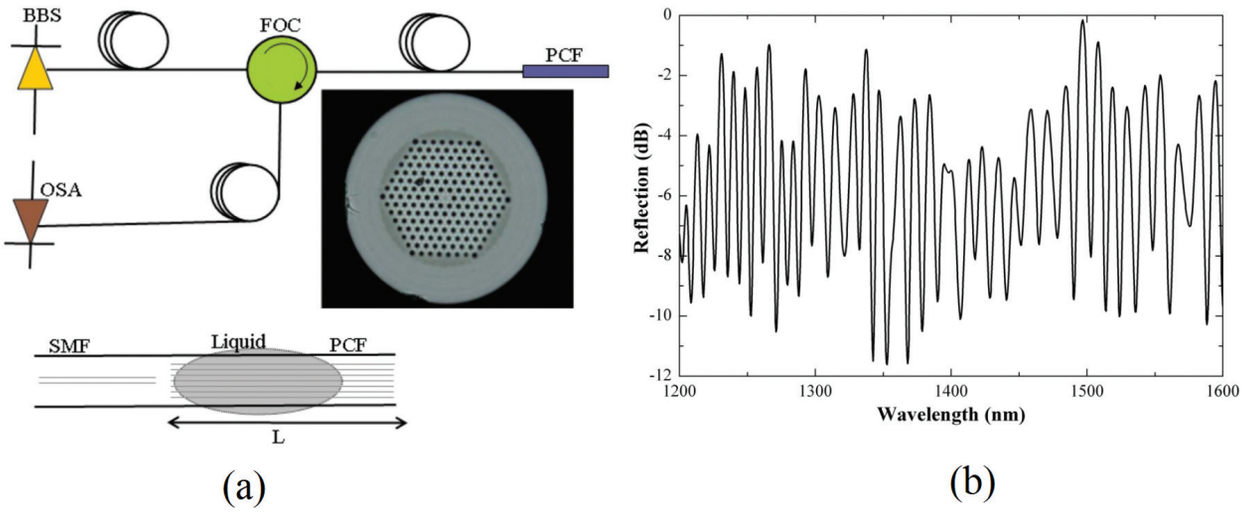

Figure 6. (a). Schematic of the experimental setup. A micrograph of the PCF used in the experiments is shown. The bottom drawing represents the interferometer, being L the length of the PCF. BBS stands for broad brand source, FOC for fiber optic circulator or coupler, and OSA for optical spectrum analyzer. (b). Reflection spectrum of a device with L = 24 mm over 400 nm. Reprinted from Ref. [58], with the permission of AIP publishing.

a section of the PCF was collapsed to excite cladding modes which possessed lower effective refractive indices than that of the core mode. The end facet of the PCF was coated with a gold film as the reflective mirror. The DNA hybridization and methylation resulted in a variation of surrounding RI, which changed the effective refractive indices of the cladding modes. The experimental results demonstrated a detection limit of 5 nM [61].

Sun et al. demonstrated a hybrid fiber interferometer by splicing a short length of PM-PCF, 177 μm, to a SMF of one output port of a 2 × 2 50:50 fiber coupler, forming a Fabry-Perot cavity in one of the optical paths of the Michelson interferometer. The spectral response of the hybrid interferometer exhibited two distinctive interference fringes and was demonstrated experimentally for simultaneous measurements of ambient RI from 1.33 to 1.38 with a resolution of 8.7×10^{-4}, and temperature in the range of 35–500°C with sensitivity of 13 pm/°C [53].

Multicore fiber (MCF) based multipath Michelson interferometers have been proposed and demonstrated for high temperature sensing recently [64]. The reflective mirror was formed via arc-fusion splicing the fiber end face. The splicing region between SMF and MCF was tapered for coupling the center core mode to surrounding cores due to reduced distances. The seven cores acted as the different optical paths in the multipath Michelson interferometer. The device demonstrated a temperature sensitivity of 165 pm/°C in the temperature range of 250–900°C [64].

Besides sensor applications, generation of logic gates such as optical add-drop multiplexers based on PCF-based Michelson interferometers has been investigated recently [54].

2.4. Sagnac interferometer

Optical fiber Sagnac interferometers (OFSI) use a Sagnac loop as the sensing element which usually uses highly birefringent (Hi-Bi) fibers or polarization-maintaining fibers (PMFs) to introduce a large optical path difference for interference between two counter-propagating waves.

The configuration of a fiber Sagnac interferometer is illustrated by **Figure 7**. The input light is split by an optical fiber coupler, usually a 3 dB coupler. Two counter-propagating waves travel in the Sagnac loop and accumulate an optical path difference due to birefringence.

Compared to conventional Hi-Bi fibers, PM-PCFs usually achieve much higher birefringence. Consequently, the required length of PM-PCF in the Sagnac loop is much shorter than that of conventional PMFs. Moreover, PM-PCFs are thermally stable due to their pure-silica material used in the fiber compared to conventional PMFs with temperature dependent birefringence. PM-PCFs also possess advantage of low bending loss due to high numerical aperture and small core diameters. As a result, PM-PCF based Sagnac interferometers have been extensively exploited and develop for many applications, such as strain, twist, pressure and curvature sensing, etc.

The temperature insensitivity of PM-PCF based Sagnac interferometers improves the accuracy of strain measurements, as the temperature crosstalk is negligible. The temperature dependence of birefringence in the PM-PCF is 35 times smaller than that of conventional PMFs [65].

Further reduced temperature sensitivities in strain measurements using PM-PCFs were reported to be 0.29 pm/K, about 3000 times lower than that of conventional PMFs, with strain sensitivity of 0.23 pm/με [66]. The experimental setup is shown in **Figure 8(a)**, consisting of a 3 dB fiber coupler to equally split the input light into two counter-propagating waves. The 86 mm long

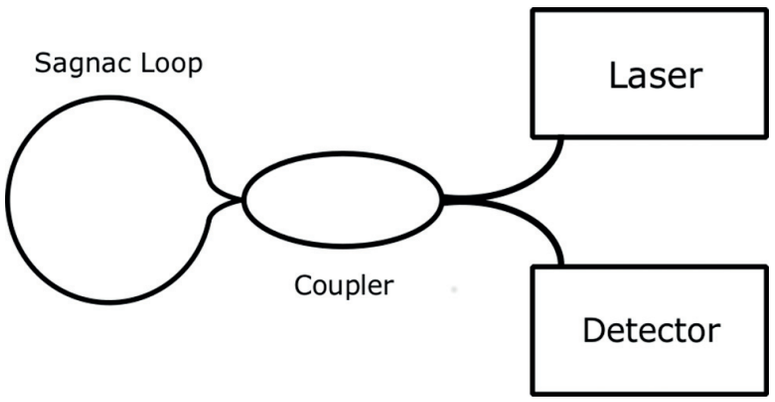

Figure 7. The schematic of a fiber Sagnac interferometer.

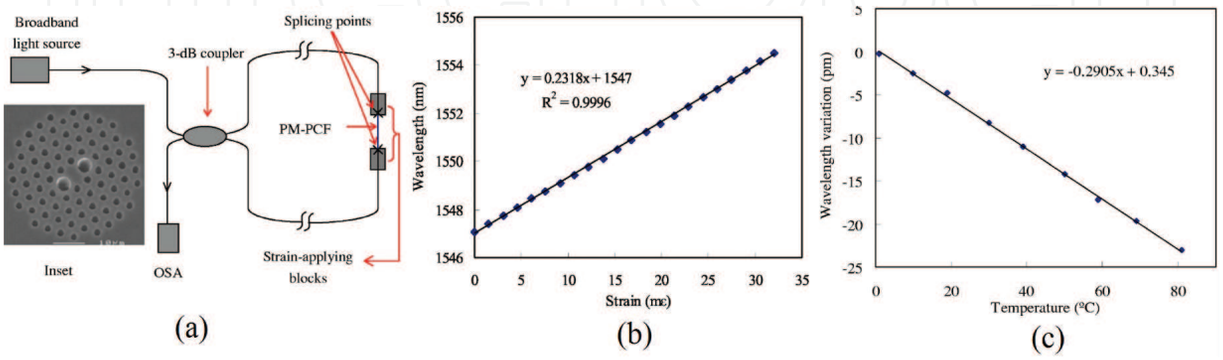

Figure 8. (a) Schematic diagram of the proposed OFSI strain sensor. Inset: SEM of the cross section of the PM-PCF. (b) wavelength shift of the transmission minimum at 1547 nm against the applied strain. (c) Wavelength variation of the transmission minimum at 1547 nm against temperature. Reprinted from Ref. [66], with the permission of AIP Publishing.

PM-PCF was spliced to the single mode fiber in the Sagnac loop. One end of the PM-PCF was fixed and the other end was stretched using a precision translation stage, for strain measurement. The scanning electron microscopic (SEM) image of the PM-PCF is shown in the inset of **Figure 8(a)**. A broadband light source is connected to the input port of the 3 dB coupler, and the transmitted light is measured by an optical spectrum analyzer (OSA) that is connected to the other input port of the 3 dB coupler. The interference occurred when two orthogonal guided modes combined at the coupler due to an accumulated phase delay in the Sagnac loop.

The transmission ratio of the optical intensity in the Sagnac loop can be described as:

$$T = [1 - \cos(\psi)]/2 \tag{5}$$

where $\psi = 2\pi LB/\lambda$ is the phase difference between the two orthogonal guided modes in PM-PCF, L is the length of the PM-PCF, B is the birefringence of the PM-PCF, and λ is the wavelength. The peak wavelength of the interference would encounter a shift due to the strain experienced by the PM-PCF, with the relationship being:

$$\Delta\lambda = \lambda\left(1 + p_e'\right)\varepsilon \tag{6}$$

where p_e' is a constant that describes the variation of strain-induced birefringence, and ε is the applied strain.

The linear relationship between strain and peak wavelength shift can be observed in **Figure 8(b)**. The temperature stability was tested by placing the PM-PCF in a temperature-controlled container, and the transmission spectrum was monitored by varying the temperature. The temperature sensitivity of the sensor was measured to be −0.29 pm/°C, as shown in **Figure 8(c)**, which is much lower than the reported value of 0.99 nm/°C of a conventional optical fiber Sagnac interferometer [67].

The influence of the coating on the fiber was investigated by Frazão et al., showing higher strain sensitivities and stronger temperature crosstalk with a nonlinear response for coated PCFs based Sagnac interferometers [68, 69]. The strain measurement sensitivities using PM-PCFs is also influenced by the ratio of the sensing PM-PCF over the entire PM-PCF length in the Sagnac loop [70]. Kim et al. develop a hollow core with an elliptical shape PBG fiber Sagnac interferometer for strain sensing with reduced temperature sensitivity when compared to conventional PMF Sagnac interferometers [71]. All-solid PCFs with Ge:SiO_2 rods and stress-induced birefringence by two Boron-doped rods have been reported to produce higher strain sensitivity of 25.6 pm/$\mu\varepsilon$ with the temperature crosstalk suppressed to −9 pm/K using a cascaded Sagnac configuration [72]. The reference signal at wavelength 1586.7 nm was used for temperature compensation of the two sensing wavelengths at 1551.5 nm and 1616.3 nm, with the wavelength difference being monitored [72]. Low-birefringence (low-Bi) PCFs with birefringence one or two orders lower than PM-PCFs were also exploited to achieve broader strain sensing range with similar strain sensitivity and a need for temperature compensation due to higher temperature sensitivity [73].

PCF-based Sagnac interferometers have been reported to develop twist or torsion sensors with potential applications in spaceflight and constructional engineering. Compared to other

optical fiber twist/torsion sensors, PCF-based Sagnac interferometers exhibit higher sensitivities and reduced crosstalk due to temperature. Hi-Bi PCFs have been reported to construct twist/torsion sensors with sensitivities 0.059 and 0.057 nm/°, as measured from two interference peaks, and temperature crosstalk of −4.6 and −2.6 pm/°C, respectively [74]. Improved twist sensitivities were obtained by using a low-Bi PCF Sagnac interferometer showing sensitivity of 1.00 nm/° and temperature sensitivity of −0.5 pm/°C [75]. A Side-leakage PCF with Ge-doped core based Sagnac interferometer was reported to achieve torsion sensitivity of 0.9354 nm/°. The temperature crosstalk was around 0.054–0.178 °/°C, which could be independently determined by using matrix method [76]. Notably, matrix method was used for simultaneously multi-parameter measurement by PCF base Sagnac interferometers also. Dong et al. introduced a core-offset technique in the splicing between the PCF and standard fibers in the Sagnac loop, and measured the wavelength variation and the transmissivity difference in order to demodulate the strain and temperature [77]. More recently, Naeem et al. demonstrated a Sagnac interferometer using Hi-Bi PCF for multi-parameter measurements. The sensor consisted of hybrid interferometry; the intra-core-mode Sagnac interference and the inter-core-mode Mach-Zehnder interference. The phase shifts due to the Sagnac and Mach-Zehnder interference were measured and used to construct the sensor matrix for torsion, strain and temperature [78].

Pressure sensing using PM-PCF based Sagnac interferometers have been reported recently. Due to the high sensitivity of Sagnac interferometry, such sensors do not require modifications for sensitivity enhancement. Furthermore, the detection scheme can be wavelength shift measurement [79, 80, 81], or phase shift measurement for extended pressure measurement range up to 2.35 MPa [82]. Feng et al. demonstrated that such sensors exhibit a good linearity of the applied pressure and can accurately measure pore water pressure [81].

Gong et al. employed a low-Bi PCF in the Sagnac loop and used wavelength shift detection for curvature sensing. The achieved curvature detection resolution was 0.059 m^{-1} [83]. Comparatively, Frazão et al. demonstrated a Hi-Bi PCF Sagnac interferometer for curvature sensing with an improved detection resolution of $(1.39 \pm 0.07) \times 10^{-5}$ m^{-1}. The measurement parameter was the group birefringence β, which was defined as $\beta = \lambda^2/\Delta\lambda L$, where λ is the central wavelength in operation, $\Delta\lambda$ is the spectral width of the interferometer, and L is the length of the Hi-Bi PCF region [84].

The presence of air holes in PCF structures permits the infiltration of substances, e.g. liquid, metal etc., to introduce additional functionalities. For instance, highly sensitive temperature sensing was reported by PCF based Sagnac interferometers filled with metal [85], selectively filled with liquid [86, 87], and partially filled with alcohol [88]. The indium-filled side hole PCF was producing a change in birefringence due to the expansion of the filler metal, resulting in a high temperature sensitivity of the sensor of −9.0 nm/°C [85]. A PBG PCF was selectively filled by high index liquid, leading to temperature dependence in the bandgap properties, as well as the Sagnac interference properties. The temperature sensitivity was about −0.4 nm/°C [88]. By selectively infiltrating water at the two larger air holes adjacent to the solid core in the PM-PCF, the Sagnac interferometer showed temperature sensitivity of 0.15 nm/°C [87]. In order to realize a low cost, reusable and reliable in-line microfluidic refractometer, Wu et al. devised a device

based on a C-shaped fiber and PCF based Sagnac interferometer [89]. The C-shape fiber and the PCF were fusion spliced to standard fibers in the Sagnac loop. The C-shape fibers provided openings for fluid to flow into and out of the PCF. The device was experimentally demonstrated for in-line fluid sensing, with high sensitivity of 6621 nm/RIU over RI range of 1.33–1.333 [89].

3. Conclusions and outlook

An overview of the different interferometric sensors, based on PCF, and their applications has been presented. The structure of PCFs is versatile and many different configurations can be achieved to produce interferometers with desirable properties such as high sensitivity, small sensor heads and good stability over time for sensing applications. PCF-based Fabry-Perot interferometers utilizing short sections of hollow core fibers, or forming microbubbles as the resonance cavities, or short sections of solid core PCFs, have been reported for measurements of various physical magnitudes, including RI, temperature, strain and pressure. PCF-based MZI configurations leverage on the enhanced flexibility in controlling waveguide properties in PCF, e.g. splicing between SMF and PCF can be used as an effective way to excite higher order modes and cladding modes in PCF, which exhibit greater sensitivity to ambient parameters compared to those in conventional fibers. In addition, the difference in the effective mode indices between the cladding modes and the core mode are greater in PCF, leading to much shorter device length and thus better robustness. PCF-based Michelson interferometers are a similar version of MZI configurations, except the presence of a reflective surface to reflect the modes which are combined at the same location of mode splitting. PCF-based Sagnac interferometers usually use Hi-Bi PCFs for developing compact and highly sensitive devices for measuring parameters such as strain, twist/torsion, curvature etc. PCFs can be combined with other fiber devices such as fiber Bragg grating or long period grating devices to achieve better sensor performance, e.g. higher sensitivity, minimizing cross-talk and simultaneous multiple parameter sensing. Inclusions of other substances into the holey structure of PCFs, bring additional functionalities and enhanced sensor performance such as temperature sensors. Moving forward, PCFs are expected for more exploitations and advancement of sensor development for various sensing applications.

Author details

Dora Juan Juan Hu[1]*, Rebecca Yen-Ni Wong[1] and Perry Ping Shum[2,3]

*Address all correspondence to: jjhu@i2r.a-star.edu.sg

1 Smart Energy and Environment Cluster, Institute for Infocomm Research, A*STAR, Singapore

2 Centre for Optical Fibre Technology, School of Electrical & Electronic Engineering, Nanyang Technological University, Singapore

3 CINTRA CNRS/NTU/THALES, UMI 3288, Research Techno Plaza, Singapore

References

[1] Lee BH, Kim YH, Park KS, Eom JB, Kim MJ, Rho BS, et al. Interferometric fiber optic sensors. Sensors. 2012;**12**(3):2467-2486. DOI: 10.3390/s120302467

[2] Knight JC. Photonic crystal fibres. Nature. 2003;**424**:847-851. DOI: 10.1038/nature01940

[3] Tian F, Sukhishvili S, Photonic Crystal DH. Fiber as a lab-in-fiber optofluidic platform. In: Cusano A, Consales M, Crescitelli A, Ricciardi A, editors. Lab-on-Fiber Technology. Springer International Publishing; Switzerland, 2014. p. 315-334. DOI: 10.1007/978-3-319-06998-2_15

[4] DJJ H, Ho HP. Recent advances in plasmonic photonic crystal fibers: Design, fabrication and applications. Advances in Optics and Photonics. 2017;**9**(2):257-314. DOI: 10.1364/AOP.9.000257

[5] Villatoro J, Zubia J. New perspectives in photonic crystal fibre sensors. Optics & Laser Technology. 2016;**78**(A):67-75. DOI: 10.1016/j.optlastec.2015.07.025

[6] Hu DJJ, Wang Y, Lim JL, Zhang T, Milenko KB, Chen Z, et al. Novel miniaturized Fabry–Perot refractometer based on a simplified hollow-core fiber with a hollow silica sphere tip. IEEE Sensors Journal. 2012;**12**(5):1239-1245. DOI: 10.1109/JSEN.2011.2167678

[7] Rao YJ, Zhu T, Yang XC, Duan DW. In-line fiber-optic etalon formed by hollow-core photonic crystal fiber. Optics Letters. 2007;**32**(18):2662-2664. DOI: 10.1364/OL.32.002662

[8] Villatoro J, Finazzi V, Coviello G, Pruneri V. Photonic-crystal-fiber-enables micro-Fabry-Perot interferometer. Optics Letters. 2009;**34**(16):2441-2443. DOI: 10.1364/OL.34.002441

[9] Favero FC, Bouwmans G, Finazzi V, Villatoro J, Pruneri V. Fabry–Perot interferometers built by photonic crystal fiber pressurization during fusion splicing. Optics Letters. 2011;**36**(21):4191-4193. DOI: 10.1364/OL.36.004191

[10] Wang Y, WD N, LC R, Hu T, Guo J, Wei H. Temperature-insensitive refractive index sensing by use of micro Fabry–Pérot cavity based on simplified hollow-core photonic crystal fiber. Optics Letters. 2013;**38**(3):269-271. DOI: 10.1364/OL.38.000269

[11] Deng M, Tang CP, Zhu T, Rao YJ, LC X, Han M. Refractive index measurement using photonic crystal fiber-based Fabry-Perot interferometer. Applied Optics. 2010;**49**(9):1593-1598. DOI: 10.1364/AO.49.001593

[12] Dash JN, Jha R. Fabry–Perot based strain insensitive photonic crystal fiber modal interferometer for inline sensing of refractive index and temperature. Applied Optics. 2015;**54**(35):10479-10486. DOI: 10.1364/AO.54.010479

[13] Favero FC, Araujo L, Bouwmans G, Finazzi V, Villatoro J, Pruneri V. Spheroidal Fabry-Perot microcavities in optical fibers for high-sensitivity sensing. Optics Express. 2012;**20**(7):7112-7118. DOI: 10.1364/OE.20.007112

[14] Ran ZL, Rao YJ, Deng HY, Liao X. Miniature in-line photonic crystal fber etalon fabricated by 157 nm laser micromachining. Optics Letters. 2007;**32**(21):3071-3073. DOI: 10.1364/OL.32.003071

[15] Shi Q, Wang Z, Jin L, Li Y, Zhang H, Lu F, et al. A hollow-core photonic crystal fiber cavity based multiplexed Fabry–Pérot interferometric strain sensor system. IEEE Photonics Technology Letters. 2008;**20**(15):1329-1331. DOI: 10.1109/LPT.2008.926948

[16] Choi HY, Park KS, Park SJ, Paek UC, Lee BH, Cho ES. Miniature fiber-optic high temperature sensor based on a hybrid structured Fabry–Perot interferometer. Optics Letters. 2008;**33**(21):2455-2457. DOI: 10.1364/OL.33.002455

[17] Du Y, Qiao X, Rong Q, Yang H, Feng D, Wang R, et al. A miniature Fabry–Pérot interferometer for high temperature measurement using a double-Core photonic crystal fiber. IEEE Sensors Journal. 2014;**14**(4):1069-1073. DOI: 10.1109/JSEN.2013.2286699

[18] Frazão O, Aref SH, Baptista JM, Santos JL, Latifi H, Fahari F, et al. Fabry–Pérot cavity based on a suspended-core fiber for strain and temperature measurement. IEEE Photonics Technology Letters. 2009;**21**(17):1229-1231. DOI: 10.1109/LPT.2009.2024645

[19] Wu C, HY F, Qureshi KK, Guan BO, Tam HY. High-pressure and high-temperature characteristics of a Fabry–Perot interferometer based on photonic crystal fiber. Optics Letters. 2011;**36**(3):412-414. DOI: 10.1364/OL.36.000412

[20] Chen X, Zhao D, Qiang Z, Lin G, Li H, Qiu Y, et al. Polarization-independent Fabry–Perot interferometer in a hole-type silicon photonic crystal. Applied Optics. 2010;**49**(30):5878-5881. DOI: 10.1364/AO.49.005878

[21] Lim JL, DJJ H, Shum PP, Wang Y. Cascaded photonic crystal fiber interferometers for refractive index sensing. IEEE Photonics Journal. 2012;**4**(4):1163-1169. DOI: 10.1109/JPHOT.2012.2205911

[22] Choi HY, Kim MJ, Lee BH. All-fiber Mach-Zehnder type interferometers formed in photonic crystal fiber. Optics Express. 2007;**15**(9):5711-5720. DOI: 10.1364/OE.15.005711

[23] Wang JN, Tang JL. Photonic crystal fiber Mach-Zehnder interferometer for refractive index sensing. Sensors. 2012;**12**(3):2983-2995. DOI: 10.3390/s120302983

[24] Villatoro J, Finazzi V, Badenes G, Pruneri V. Highly sensitive sensors based on photonic crystal fiber modal interferometers. Journal of Sensors. 2009;**2009**:1-11. DOI: 10.1155/2009/747803

[25] Zheng J, Yan P, Yu Y, Ou Z, Wang J, Chen X, et al. Temperature and index insensitive strain sensor based on a photonic crystal fiber inline Mach–Zehnder interferometer. Optics Communications. 2013;**297**:7-11. DOI: 10.1016/j.optcom.2013.01.063

[26] Zhao Y, Li XG, Cai L, Refractive YY. Index sensing based on photonic crystal fiber interferometer structure with up-tapered joints. Sensors and Actuators B: Chemical. 2015;**221**:406-410. DOI: 10.1016/j.snb.2015.06.148

[27] Wang Q, Kong L, Dang Y, Xia F, Zhang Y, Zhao Y, et al. High sensitivity refractive index sensor based on splicing points tapered SMF-PCF-SMF structure Mach-Zehnder mode interferometer. Sensors and Actuators B: Chemical. 2016;**225**:213-220. DOI: 10.1016/j.snb.2015.11.047

[28] Wu D, Zhao Y, Li J. PCF taper-based Mach–Zehnder interferometer for refractive index sensing in a PDMS detection cell. Sensors and Actuators B: Chemical. 2015;**213**:1-4. DOI: 10.1016/j.snb.2015.02.080

[29] Wong WC, Zhou W, Chan CC, Dong X, Leong KC. Cavity ringdown refractive index sensor using photonic crystal fiber interferometer. Sensors and Actuators B: Chemical. 2012;**161**(1):108-113. DOI: 10.1016/j.snb.2011.09.056

[30] Liang H, Zhang W, Wang H, Geng P, Zhang S, Gao S, et al. Fiber in-line Mach–Zehnder interferometer based on near-elliptical core photonic crystal fiber for temperature and strain sensing. Optics Letters. 2013;**38**(20):4019-4021. DOI: 10.1364/OL.38.004019

[31] Geng Y, Li X, Tan X, Deng Y, Hong X. Compact and ultrasensitive temperature sensor with a fully liquid-filled photonic crystal fiber Mach–Zehnder interferometer. IEEE Sensors Journal. 2014;**14**(1):167-170. DOI: 10.1109/JSEN.2013.2279537

[32] Zhao Z, Tang M, Fu S, Liu S, Wei H, Cheng Y, et al. All-solid multi-core fiber-based multipath Mach–Zehnder interferometer for temperature sensing. Applied Physics B. 2013;**112**(4):491-497. DOI: 10.1007/s00340-013-5634-8

[33] Qureshi KK, Liu Z, Tam HY, Zia MF. A strain sensor based on in-line fiber Mach–Zehnder interferometer in twin-core photonic crystal fiber. Optics Communications. 2013;**309**:68-70. DOI: 10.1016/j.optcom.2013.06.057

[34] LM H, Chan CC, Dong XY, Wang YP, Zu P, Wong WC, et al. Photonic crystal fiber strain sensor based on modified Mach–Zehnder interferometer. IEEE Photonics Journal. 2012;**4**(1):114-118. DOI: 10.1109/JPHOT.2011.2180708

[35] Shin W, Lee YL, BA Y, Noh YC, Ahn TJ. Highly sensitive strain and bending sensor based on in-line fiber Mach–Zehnder interferometer in solid core large mode area photonic crystal fiber. Optics Communications. 2010;**283**(10):2097-2101. DOI: 10.1016/j.optcom.2010.01.008

[36] Kim B, Kim TH, Cui L, Chung Y. Twin core photonic crystal fiber for in-line Mach-Zehnder interferometric sensing applications. Optics Express. 2009;**17**(18):15502-15507. DOI: 10.1364/OE.17.015502

[37] Sun B, Huang V, Liu S, Wang C, He J, Liao C, et al. Asymmetrical in-fiber Mach-Zehnder interferometer for curvature measurement. Optics Express. 2015;**23**(11):14596-14602. DOI: 10.1364/OE.23.014596

[38] Deng M, Tang CP, Zhu T, Rao YJ. Highly sensitive bend sensor based on Mach–Zehnder interferometer using photonic crystal fiber. Optics Communications. 2011;**284**(12):2849-2853. DOI: 10.1016/j.optcom.2011.02.061

[39] Tao C, Wei H, Feng W. Photonic crystal fiber in-line Mach-Zehnder interferometer for explosive detection. Optics Express. 2016;**24**(3):2806-2817. DOI: 10.1364/OE.24.002806

[40] Lopez-Torres D, Elosua C, Villatoro J, Zubia J, Rothhardt M, Schuster K, et al. Photonic crystal fiber interferometer coated with a PAH/PAA nanolayer as humidity sensor. Sensors and Actuators B: Chemical. 2017;**242**:1065-1072. DOI: 10.1016/j.snb.2016.09.144

[41] Hu P, Dong X, Wong WC, Chen LH, Ni K, CC C. Photonic crystal fiber interferometric pH sensor based on polyvinyl alcohol/polyacrylic acid hydrogel coating. Applied Optics. 2015;**54**(10):2647-2652. DOI: 10.1364/AO.54.002647

[42] Dash JN, Jha R, Temperature Insensitive PCF. Interferometer coated with graphene oxide tip sensor. IEEE Photonics Technology Letters. 2016;**28**(9):1006-1009. DOI: 10.1109/LPT.2016.2522979

[43] DJJ H, Lim JL, Park MK, Kao LTH, Wang Y, Wei H, et al. Photonic crystal fiber-based interferometric biosensor for streptavidin and biotin detection. IEEE Journal of Selected Topics in Quantum Electronics. 2012;**18**(4):1293-1297. DOI: 10.1109/JSTQE.2011.2169492

[44] Lim JH, Jang HS, Lee K, KJ C, Lee BH. Mach–Zehnder interferometer formed in a photonic crystalfiber based on a pair of long-period fiber gratings. Optics Letters. 2004;**29**(4):346-348. DOI: 10.1364/OL.29.000346

[45] Yu X, Shum P, Dong X. Photonic-crystal-fiber-based Mach–Zehnder interferometer using long-period gratings. Microwave and Optical Technology Letters. 2006;**48**(7):1379-1383. DOI: 10.1002/mop.21647

[46] Choi HY, Park KS, Lee BH. Photonic crystal fiber interferometer composed of a long period fiber grating and one point collapsing of air holes. Optics Letters. 2008;**33**(8):812-814. DOI: 10.1364/OL.33.000812

[47] Ju J, Jin W, Ho HL. Compact in-fiber interferometer formed by long-period gratings in photonic crystal fiber. IEEE Photonics Technology Letters. 2008;**20**(23):1899-1901. DOI: 10.1109/LPT.2008.2005207

[48] Hu DJJ, Lim JL, Jiang M, Wang Y, Luan F, Shum PP, et al. Long period grating cascaded to photonic crystal fiber modal interferometer for simultaneous measurement of temperature and refractive index. Optics Letters. 2012;**37**(12):2283-2285. DOI: 10.1364/OL.37.002283

[49] Pawar D, Rao CN, Choubey RK, Kale SN. Mach-Zehnder interferometric photonic crystal fiber for low acoustic frequency detections. Applied Physics Letters. 2016;**108**(4):041912-1-041912-4. DOI: 10.1063/1.4940983

[50] Du J, Dai Y, Lei GKP, Tong W, Shu C. Photonic crystal fiber based Mach-Zehnder interferometer for DPSK signal demodulation. Optics Express. 2010;**18**(8):7917-7922. DOI: 10.1364/OE.18.007917

[51] Gerosa RM, Spadoti DH, Menezes LS, de Matos CJS. In-fiber modal Mach-Zehnder interferometer based on the locally post-processed core of a photonic crystal fiber. Optics Express 2011;**19**(4):3124-3129. DOI: 10.1364/OE.19.003124

[52] Tan X, Geng Y, Li X. High-birefringence photonic crystal fiber Michelson interferometer with cascaded fiber Bragg grating for pressure and temperature discrimination. Optical Engineering. 2016;**55**(9):090508. DOI: 10.1117/1.OE.55.9.090508

[53] Sun H, Zhang J, Rong Q, Feng D, Du Y, Zhang X, et al. A hybrid fiber interferometer for simultaneous refractive index and temperature measurements based on Fabry–Perot/ Michelson interference. IEEE Sensors Journal. 2013;**13**(5):2039-2044

[54] Sousa JRR, Filho AFGF, Ferreira AC, Batista GS, Sobrinho CS, Bastos AM, et al. Generation of logic gates based on a photonic crystal fiber Michelson interferometer. Optics Communications. 2014;**322**:143-149. DOI: 10.1016/j.optcom.2014.02.023

[55] Zhou A, Li G, Zhang Y, Wang Y, Guan C, Yang J, et al. Asymmetrical twin-Core fiber based Michelson interferometer for refractive index sensing. Journal of Lightwave Technology. 2011;**29**(19):2985-2991. DOI: 10.1109/JLT.2011.2165528

[56] Chen NK, KY L, Shy JT, Lin C. Broadband micro-Michelson interferometer with multi-optical-path beating using a sphered-end hollow fiber. Optics Letters. 2011;**36**(11):2074-2076. DOI: 10.1364/OL.36.002074

[57] Hu DJJ, Lim JL, Wang Y, Shum PP. Miniaturized photonic crystal fiber tip sensor for refractive index sensing. In: Proceedings of the IEEE Sensors Conference; 28-31 October 2011; Limerick, Ireland: IEEE; 2011. p. 1488-1490

[58] Jha R, Villatoro J, Badenes G. Ultrastable in reflection photonic crystal fiber modal interferometer for accurate refractive index sensing. Applied Physics Letters. 2008;**93** (19):191106. DOI: 10.1063/1.3025576

[59] Mileńko K, Hu DJJ, Shum PP, Zhang T, Lim JL, Wang Y, et al. Photonic crystal fiber tip interferometer for refractive index sensing. Optics Letters. 2012;**37**(8):1373-1375. DOI: 10.1364/OL.37.001373

[60] Hsu JM, Horng JS, Hsu CL, Lee CL. Fiber-optic Michelson interferometer with high sensitivity based on a liquid-filled photonic crystal fiber. Optics Communications. 2014;**331**:348-352. DOI: 10.1016/j.optcom.2014.06.050

[61] Gao R, DF L, Cheng J, Jiang Y, Jiang L, JD X, et al. Fiber optofluidic biosensor for the label-free detection of DNA hybridization and methylation based on an in-line tunable mode coupler. Biosensors & Bioelectronics. 2016;**86**:321-329. DOI: 10.1016/j.bios.2016.06.060

[62] Gong H, Chan CC, Zhang YF, Wong WC, Dong X. Miniature refractometer based on modal interference in a hollow-core photonic crystal fiber with collapsed splicing. Journal of Biomedical Optics. 2011;**16**(1):017004. DOI: 10.1117/1.3527259

[63] Li Z, Wang Y, Liao C, Liu S, Zhou J, Zhong X, et al. Temperature-insensitive refractive index sensor based on in-fiber Michelson interferometer. Sensors and Actuators B: Chemical. 2014;**199**:31-35. DOI: 10.1016/j.snb.2014.03.071

[64] Duan L, Zhang P, Tang M, Wang R, Zhao Z, Fu S, et al. Heterogeneous all-solid multicore fiber based multipath Michelson interferometer for high temperature sensing. Optics Express. 2016;**24**(18):20210-20218. DOI: 10.1364/OE.24.020210

[65] Kim DH, Kang JU. Sagnac loop interferometer based on polarization maintaining photonic crystal fiber with reduced temperature sensitivity. Optics Express. 2004;**12**(19):4490-4495. DOI: 10.1364/OPEX.12.004490

[66] Dong X, Tam HY, Shum P. Temperature-insensitive strain sensor with polarization-maintaining photonic crystal fiber based Sagnac interferometer. Applied Physics Letters. 2007;**90**(15):151113. DOI: 10.1063/1.2722058

[67] Starodumov AN, Zenteno LA, Monzon D, Rosa EDL. Fiber Sagnac interferometer temperature sensor. Applied Physics Letters. 1997;**70**(1):19. DOI: 10.1063/1.119290

[68] Frazao O, Baptista JM, Santos JL. Temperature-independent strain sensor based on a Hi-Bi photonic crystal fiber loop mirror. IEEE Sensors Journal. 2007;**7**(10):1453-1455. DOI: 10.1109/JSEN.2007.904884

[69] Frazao O, Baptista JM, Santos JL, Kobelke J, Schuster K. Strain and temperature characterisation of sensing head based on suspended-core fibre in Sagnac interferometer. Electronics Letters. 2008;**44**(25):1455-1456. DOI: 10.1049/el:20081431

[70] Cui Y, Wu Z, Shum PP, Dinh XQ, Humbert G. Investigation on the impact of Hi-Bi fiber length on the sensitivity of Sagnac interferometer. IEEE Sensors Journal. 2014;**14**(6):1952-1956. DOI: 10.1109/JSEN.2014.2304521

[71] Kim G, Cho T, Hwang K, Lee K, Lee KS, Han YG, et al. Strain and temperature sensitivities of an elliptical hollow-core photonic bandgap fiber based on Sagnac interferometer. Optics Express. 2009;**17**(4):2481-2486. DOI: 10.1364/OE.17.002481

[72] Gu B, Yuan W, He S, Bang O. Temperature compensated strain sensor based on cascaded Sagnac interferometers and all-solid Birefringent hybrid photonic crystal fibers. IEEE Sensors Journal. 2012;**12**(6):1641-1646. DOI: 10.1109/JSEN.2011.2175725

[73] Gong H, Chan CC, Chen L, Dong X. Strain sensor realized by using low-birefringence photonic-crystal-fiber-based Sagnac loop. IEEE Photonics Technology Letters. 2010;**22**(16):1238-1240. DOI: 10.1109/LPT.2010.2053025

[74] Kim HM, Kim TH, Kim B, Chung Y. Temperature-insensitive torsion sensor with enhanced sensitivity by use of a highly birefringent photonic crystal fiber. IEEE Photonics Technology Letters. 2010;**22**(20):1539-1541. DOI: 10.1109/LPT.2010.2068043

[75] Zu P, Chan CC, Jin Y, Gong T, Zhang Y, Chen LH, et al. A temperature-insensitive twist sensor by using low-birefringence photonic-crystal-fiber-based Sagnac interferometer. IEEE Photonics Technology Letters. 2011;**23**(13):920-922. DOI: 10.1109/LPT.2011.2143400

[76] Chen W, Lou S, Wang L, Zou H, Lu W, Jian S. Highly sensitive torsion sensor based on Sagnac interferometer using side-leakage photonic crystal fiber. IEEE Photonics Technology Letters. 2011;**23**(21):1639-1641. DOI: 10.1109/LPT.2011.2166062

[77] Dong B, Hao J, Chin-Yi L, Xu Z. Cladding-mode resonance in polarization-maintaining photonic-crystal-fiber-based Sagnac interferometer and its application for fiber sensor. Journal of Lightwave Technology. 2011;**29**(12):1759-1763. DOI: 10.1109/JLT.2011.2140313

[78] Naeem K, Kim BH, Kim B, Chung Y. Simultaneous multi-parameter measurement using Sagnac loop hybrid interferometer based on a highly birefringent photonic crystal fiber with two asymmetric cores. Optics Express. 2015;**23**(3):3589-3601. DOI: 10.1364/OE.23.003589

[79] HY F, Tam HY, Shao LY, Dong X, Wai PKA, Lu C, et al. Pressure sensor realized with polarization-maintaining photonic crystal fiber-based Sagnac interferometer. Applied Optics. 2005;**47**(15):2835-2839. DOI: 10.1364/AO.47.002835

[80] HY F, Wu C, Tse MLV, Zhang L, Cheng KCD, Tam HY, et al. High pressure sensor based on photonic crystal fiber for downhole application. Applied Optics. 2010;**49**(14):2639-2643. DOI: 10.1364/AO.49.002639

[81] Feng WQ, Liu ZY, Tam HY, Yin JH. The pore water pressure sensor based on Sagnac interferometer with polarization-maintaining photonic crystal fiber for the geotechnical engineering. Measurement. 2016;**90**:208-214. DOI: 10.1016/j.measurement.2016.04.067

[82] Cho LH, Wu C, Lu C, Tam HY. A highly sensitive and low-cost Sagnac loop based pressure sensor. IEEE Sensors Journal. 2013;**13**(8):3073-3078. DOI: 10.1109/JSEN.2013.2261291

[83] Gong HP, Chan CC, Zu P, Chen LH, Dong XY. Curvature measurement by using low-birefringence photonic crystal fiber based Sagnac loop. Optics Communications. 2010;**283**(16):3142-3144. DOI: 10.1016/j.optcom.2010.04.023

[84] Frazão O, Baptista JM, Santos JL, Roy P. Curvature sensor using a highly birefringent photonic crystal fiber with two asymmetric hole regions in a Sagnac interferometer. Applied Optics. 2008;**47**(13):2520-2523. DOI: 10.1364/AO.47.002520

[85] Reyes-Vera E, Cordeiro CMB, Torres P. Highly sensitive temperature sensor using a Sagnac loop interferometer based on a side-hole photonic crystal fiber filled with metal. Applied Optics. 2017;**56**(2):156-162. DOI: 10.1364/AO.56.000156

[86] Zheng X, Yg L, Wang Z, Han T, Wei C, Chen J. Transmission and temperature sensing characteristics of a selectively liquid-filled photonic-bandgap-fiber-based Sagnac interferometer. Applied Physics Letters. 2012;**100**(14):141104. DOI: 10.1063/1.3699026

[87] Cui Y, Shum PP, Hu DJJ, Wang G, Humbert G, Dinh XQ. Temperature sensor by using selectively filled photonic crystal fiber Sagnac interferometer. IEEE Photonics Journal. 2012;**4**(5):1801-1808. DOI: 10.1109/JPHOT.2012.2217945

[88] Zhao CL, Wang Z, Zhang S, Li Q, Zhong C, Zhang Z, et al. Phenomenon in an alcohol not full-filled temperature sensor based on an optical fiber Sagnac interferometer. Optics Letters. 2012;**37**(22):4789-4791. DOI: 10.1364/OL.37.004789

[89] Wu C, Tse MLV, Liu Z, Guan BO, Lu C, Tam HY. In-line microfluidic refractometer based on C-shaped fiber assisted photonic crystal fiber Sagnac interferometer. Optics Letters. 2013;**38**(17):3283-3286. DOI: 10.1364/OL.38.003283

IntechOpen